行政院原子能委員會

委託研究計畫研究報告

【應用於太陽能轉換之量子點敏化 InN/TiO_2 奈米粒子薄膜研發】

【Quantum-Dot Enhanced InN/TiO_2 Nanoparticle Films for Solar Energy Conversion Applications】

計畫編號：962001 INER 0029

受委託機關(構)：國立交通大學

計畫主持人：林明璋

核研所參與人員：藍山明、陳盈汝

聯絡電話：(03)5731696

E-mail address：chemmcl@emory.edu

報告日期：96 年 11 月 23 日

目　錄

中文摘要

本計畫是為期四年行政院原子能委員會委託研究計畫之第三年執行結果摘要。本年的主要工作在進行以下目標：(一)利用 plasma-enhanced 及 organometallic chemical vapor deposition (PECVD 及 OMCVD)的方法完成第一階段製作 InN/TiO_2 量子點太陽電池，結果與去年 NREL 之 Nozik 認為有相當高效率的 InAs/TiO_2 量子點太陽電池效率近似；(二)完成 InN/-OB(O)O/TiO_2 及 InN/OP(O)O/TiO_2 系統之聯鍵（-OY(O)O-, Y=B 及 P）效率的比較，前者有明顯的效率增加，而後者明顯的降低，此結果顯示化性強壯的 HOB(O)O 化學鍵可利用為其他半導體量子點接連 TiO_2 奈米薄膜的主要工具(諸如 CdSe, Si, Ge, ZnO 等）。

此外，一系列的半導體量子點(QD)及奈米粒子(NP)亦用水熱法製作，諸如 ZnO, M-doped ZnO (M=Fe, Co), In_2O_3 及 InTe. 此類 QD 及 NP 將可利用為 InN/QD(NP)/TiO_2 的介面導電物質。

未來一年將在新的 In(M)N/Linker/d-TiO_2 奈米光電系統逐步改進三構件(components)：(1)敏化量子點 InN 加入不同的 dopants (M=Ga, Al, Zn, Sb…)；(2)化學聯結鍵(Linker), -OY(O)O < (Y=B, P, Al, Si, Zn...)的變化應用；及(3) TiO_2 奈米基板加入 dopants (d=B, P, Zn, W…)，有系統的調製三構件，配合飛秒雷射作電子轉移動態的測量，期以導致一件高效率、化性物性堅牢的太陽電池，供給水分解的應用。

Abstract

This is the report for the third year of the 4-year proposal on the III-V metal nitride nanoparticle-enchanced TiO_2 solar cell, initially focussing on the InN/TiO_2 nanoparticle system.

In the proposed studies at NCTU, our emphasis has been placed primarily on the development of an economically viable solar energy conversion system for photovoltaic and, most importantly, for photo-electrochemical water-splitting applications. The low-cost, nontoxic and chemically and thermally stable properties of TiO_2 have resulted in much recent research effort to circumvent its large band gap (3.2 eV or 387 nm) by modifying its surface optical properties for applications in the visible region of the spectrum, specifically for solar energy conversion. The best known technique to enhance its photovoltaic efficiency is Graetzel's method using dyes to improve its photo-absorption cross section and electron transfer dynamics.

The best dye employed by Graetzel and co-workers, $RuL(SCN)_3$, has reached ~10% solar energy conversion efficiency under their best operational conditions. It is comparable to amorphous silicon systems with 9-10% efficiencies and is less than that of polycrystalline silicon devices which have been reported to reach >15% efficiency. It should be noted that both the organic dye/TiO_2 and polycrystalline Si systems are costly and still cannot compete economically with fossil fuels such as coals and natural gases.

In the past year, we have completed the first phase of InN/TiO_2 employing two different InN deposition techniques, PECVD (Plasma enhanced chemical vapor deposition) and OMCVD (organometallic

CVD) using the TiO_2 nanoparticle films prepared by the common sol gel method. The fabricated InN/TiO_2 devices by both methods have now reached the best device fabricated by Nozik et al. of NREL published last year.

In another series of experiments, we have achieved a critical milestone by carefully analyzing the effects of $B(OH)_3$ vs $P(OH)_3$ as linkers between InN and TiO_2. The results indicate clearly that the –OB(O)O-anchoring group enhances the InN/TiO_2 photocurrent, whereas the –OP(O)P-group pronouncedly reduces the photocurrent. The theoretical underpinning of this critical finding is currently under quantum-chemical study on their binding characteristics.

In addition to these important milestones, we have continued the syntheses of a variety of semiconductor quantum dots for future incorporation into the interface between InN and TiO_2, for example, $InTe_x$, ZnO and M-ZnO (M=Fe, Co, etc.). Once the cavities of the top layer TiO_2 nanoparticle films can be effectively increased and enlarged, these QDs will be employed for the fabrication of $InN/QD/TiO_2$ devices.

壹、計畫緣起與目的

由於天然能源的缺乏，台灣每年約有 98 %的能源仰賴進口。因此，台灣應該優先地投資在再生能源的研究領域。在此科學領域中，台灣已遠遠落後於日本、美國和歐洲。太陽是一個取之不盡、用之不竭的天然資源，因此有效率地使用太陽能應是二十一世紀最重要的科技挑戰之一。

此計畫將在交通大學執行，但和核能所密切合作。我們主要著重於發展一個具經濟效益的太陽能轉換系統以應用在太陽能光電轉換及/或光電化學上分解水的研究。二氧化鈦(TiO_2)的低成本、無毒性、及化學及熱穩定的性質，使得相當多的研究群組致力於研究如何透過表面光學特性的修飾以克服其較大的 band gap（3.2 eV 或 387 nm），以將其應用於可見光區，尤其是太陽能之轉換。而提升其光電效率的最著名的技術乃是 Graetzel's 所發展出以染料改進半導體之光吸收截面積及電子轉移動態學的方法。

Graetzel 等人使用最理想的染料，在最佳的實驗條件下，已可達到 10 %的太陽能轉換效益，其轉換效益和非晶形矽系統的 9-10 % 相當，但比多晶形矽系統的>15 %差。值得注意的是，有機染料/TiO_2 及多晶形矽系統之成本尚高，其經濟效益仍然無法與石化燃料，如與石碳及天然氣相比。

於是我們希望可以利用半導體量子點取代有機染料，改善其不穩定的缺點。在半導體量子點敏化的研究中，選用矽、氮化鋁及其他半導體或導體作為吸收太陽能的敏化物。矽及氮化鋁量子點的能隙依其粒子大小而定，大約是 1.6 ev 左右，可以吸收太陽光中大

量的輻射能量(太陽光中已可見光及紅外光含量最多)。

在 Emory 大學，林明璋研究組已經成功地利用低壓有機金屬化學蒸鍍法（OMCVD），使用 HN_3 及 $In(CH_3)_3$，將所產生的 InN 薄膜沈積在已吸附固定於 sapphire 片或 Ti 金屬上之 TiO_2 奈米粒子上[1]。此沈積的 InN/TiO_2 奈米粒子薄膜呈現非常寬廣的 390-800 nm 紫外/可見光吸收譜帶，其吸收光區與 Graetzel [2] 等人的 black dye/TiO_2 系統所量測的結果相當類似。此半導體的 InN/TiO_2 薄膜其穩定的化學性質或許有助於其利用於光電轉率及水分解應用上的耐用性。在後者的應用上，已有類似但昂貴的方法使用 InGaP/GaAs 光電極可達到令人印象深刻的 12.4 %轉換效率[3]。相較於 InGaP/GaAs 系統在光電化學之應用上，InN/TiO_2 奈米粒子薄膜其化性較穩定且製造成本更便宜。

InN/TiO_2 奈米薄膜在光電轉換之電子轉移等物理特性將利用交通大學的超快雷射技術來研究，而其光電子產生及轉移的效率則可以利用光電流的直接量測而得到。在台灣，超快雷射技術應用於凝態的研究，交通大學應用化學系居於領先之地位。

除了我們所量測到增強的 InN/TiO_2 薄膜在紫外/可見光區吸收，最近 Nozik 等人已經偵測到以 InP 及 InAs 量子點吸附在 TiO_2 奈米薄膜上，其在紫外/可見光區之吸收有顯著的提升[4,5]。由於物理吸附之作用力通常不強，且 InP 及 InAs 不夠耐用，所以 Nozik 的 InX/TiO_2 (X=P, As)系統大概無法長久的使用，尤其在溶液中使用。因此，是否可以利用有機金屬蒸鍍法以一層化性穩定之 InN 薄膜，將這些量子點包覆起來？若可以這麼做，這些以 InN 包覆的 InX 量子點或其他類似的高效率光電轉換材料所產生的光電子是否能有效

率地轉移到 TiO_2 上？這些是我們在發展一個有效率和具經濟效益的光電轉換及水分解系統的過程中，希望能有系統來探討的問題。

在此計畫中，我們擬議研究以 InN 奈米粒子或薄膜覆蓋其他半導體奈米粒子的效應。最初，我們將研究嵌入 Si, InP 及其他半導體兩種量子點在 InN 和 TiO_2 奈米薄膜之間，如前所述。Si 和 InP 均具有相似之能隙(分別為 1.1 與 1.3 eV)。除此之外，我們將以其他金屬氧化物之量子點或奈米粒子修飾 TiO_2 基版，以改變 TiO_2 的能帶邊(band edge)，使其與 InN 奈米薄膜或量子點的重疊變為最大。除此以外，InN 及 TiO_2 之間的接連化學鍵及 TiO_2 奈米薄膜的 dopant 效應(諸如 n-或 p- dopant 影響光電效應)的研究，亦為未來本計劃的研發重點。

References:

1. J. H. Wang and M. C. Lin, ChemPhysChem, 2004, 5, 1615.
2. A. Hagfeld, M. Graetzel, Chem. Rev., 1995, 95, 49; M. K. Nazeeruddin, P. Pechy, M. Graetzel, Chem. Comm., 1997, 18, 1705; M. Graetzel, Nature, 2001, 414, 338.
3. O. Khaselev and J. A. Turner, Science, 1998, 280, 425.
4. Zaban, O. I. Mic´ic´, B. A. Gregg, A. J. Nozik, Langmuir, 1998, 14, 3153-3156; J. M. Nedeljkovic´, O. I. Mic´ic´, S. P. Ahrenkiel, A. Miedaner, A. J. Nozik , J. Am. Chem. Soc., 2004, 126, 2632-2639.
5. P. Yu, K Zhu, A. G. Norman, S. Ferrere, A. J. Frank and A. J. Nozk, J. Phys. Chem. B, 2006, 110, 25451.

貳、研究方法與過程

一、Preparation of semiconductor nanoparticles（C. S. Lee）:

Synthesis of Metal Chalcogenide and Metal Oxide Nanoparticles

The goals of this project are to prepare and characterize new semiconductor and metal oxide nanoparticles to fabricate thin film electrode for solar cell applications. This report covers the time period of January 1 - December 31, 2007. Several nanomaterials have been synthesized and tested include: 1) Au incorporated $In(OH)_3$ and In_2O_3: A new synthetic route to grow $In(OH)_3$ and In_2O_3 nanocrystals of rectangular shape and incorporating Au is presented. The elemental Au is deposited on the surface of $In(OH)_3$ rectangular nanocrystals as a thin film and incorporated into In_2O_3 nanoporous material as nanoparticles. 2) Morphology controlled $Co_xZn_{1-x}O$: A systematic approach to synthesize Co^{2+} doped ZnO nanocrystals with controlled particle shape has been developed. The Co^{2+} doped ZnO exhibit strong absorption in visible light region, which could affect the photo energy conversion of metal oxide film made up of Co-ZnO nanoparticles. 3) InTe nanoparticles on TiO_2 film: the influence of the InTe quantum dot on photovoltaic performance was observed with best efficiency of 0.134% under illumination by simulated AM 1.5 solar light (100 mW/cm^2). During this year six conference posters were presented. [1-6]

Materials with confined structures have attracted much research, especially metal oxides incorporating metal nanoparticles that are potentially useful for applications including catalysts, photocatalysts, solar cells etc. Among such reported materials, ZnO,

$In(OH)_3$ and In_2O_3 are of particular interest due to their peculiar physical properties.[7-9] They are both wide band-gap semiconductors. A thin film of $In(OH)_3$ exhibits conductivity in a range 10^{-7}–10^{-3} S/cm^2 and In_2O_3 nanomaterials show satisfactory electrical conductivity and a high sensitivity towards some gases. ZnO is a wide band-gap semiconductor which doping with transition metal impurities has been widely investigated as a strategy for extending the photo responses into the visible spectral range, thereby making them suitable candidates for photochemical conversion of solar energy into electrical or chemical potential. For low band gap semiconducting materials, it has been considered as the alternative source of sensitizer for solar cell device. Our studies have been focused on the preparation of semiconductor nanomaterials in varies binary systems and TiO_2 anatase nanoparticle films. As these metal-incorporating oxide materials are prospectively applicable for solar cell, our research has focused on discovering new synthetic routes to deposit a metal element or semiconductor nanoparticles on metal-oxide nanoparticles to assemble thin film electrode for solar cell. In this report, we report the synthesis and optic property studies of Au-doped $In(OH)_3/In_2O_3$ nanoparticles, Co:ZnO nanoparticle with controlled shape, and $InTe/TiO_2$ film.

Experimental

1. Synthesis

(1) Synthesis of $In(OH)_3$ and In_2O_3: In a typical experiment, sodium hydroxide solution (10 M, 72 mL) was added dropwise to $InCl_3$ solution (0.3 g, 1.35 mmol) under vigorous stirring at 23 °C. The milky-white colloid suspension was subjected to

vigorous stirring and sonic treatment for at least 30 min before being transferred to a Teflon-lined stainless-steel autoclave (capacity 23 mL) and heated at 160 °C for 20 h. The white precipitate of $In(OH)_3$ was washed thoroughly with DI water under ultrasonic condition (240W output), centrifuged and finally dried in vacuum to collect the product. Nanoporous In_2O_3 shows a light yellow color, obtained on calcination of $In(OH)_3$ in a crucible at a temperature 450 °C and maintained in air for 2 h.

(2) Synthesis of Au-incorporating $In(OH)_3$ and In_2O_3: A sodium hydroxide solution (72 mL, 10 M) was added dropwise to $InCl_3$ (0.3 g, 1.35 mmol) under vigorous stirring at 23 °C, followed by slow addition of $HAuCl_4$ solution (5 %) until the molar ratio Au/In =1. The light yellow solution was subjected to vigorous stirring and sonic treatment for at least 30 min before being transferred to a Teflon-lined stainless-steel autoclave (capacity 23 mL) and heated at 160 °C for 20 h. The violet-red precipitate was washed thoroughly with DI water under ultrasonic conditions (240 W output), then centrifuged and finally dried in vacuum to collect the product of Au-$In(OH)_3$. The powder as prepared was calcined in a crucible at a temperature 450 °C and maintained for 2 h in air to form Au-incorporating In_2O_3 with a similar violet-red color.

(3) Synthesis of ZnO nanorods on ITO film[9]: A thin film of zinc oxide was coated on the ITO substrate by doctor blade method (thickness ~ 5um) with a solution containing nanoparticles of zinc oxides. ZnO nanoparticles were prepared by

(6) Synthesis of InTe Nanoparticles: InTe nanoparticles were prepared by mixing a solution of $InCl_3$, Te element in solution of trioctylphosphine (TOP). The mixed solution was heated for 2 – 60 min at 180 °C under nitrogen atmosphere. Formation of the InTe nanoparticles is accompanied by the appearance of an intense dark brown color. The as synthesized nanoparticles were diluted with toluene and precipitated with methanol. The precipitate was dissolved in pyridine and precipitated again in an excess amount of methanol. The resulting black suspensions were centrifuged and the precipitates were washed three times with absolute methanol. The as synthesized nanoparticles were diluted with toluene and precipitated with methanol. The precipitate was dissolved in pyridine and precipitated again in excess amount of methanol.

2. Characterization

XRD, UV, PL, SEM, TEM, TGA, BET: The product as prepared was characterized by XRD (Bruker AXS D8 Advance, Leipzig Germany, Cu Kα radiation at 40 kV and 40 mA), SEM (Hitachi, S-4700I, operated at 15kV), TEM (JEOL, JEM-3000F, operated at 200 kV), UV-vis absorption spectra (Hitachi, U-3010 spectrometer, scanning wavelength 190 nm~1000 nm, Al_2O_3 plate as reference), thermogravimetric analyis (TGA, Perkin-Elmer Pyris, T = 50 - 750°C, rate 10 °C/min), and PL measurements (Jobin-Yvon Spex Fluorolog-3, λex = 365 nm, filter wavelength = 400 nm, Xe lamp, 23 °C, scanning wavelength 400 - 800nm). Surface areas were determined by the BET method from the adsorption of nitrogen at 77 K with a

surface area analyzer (NOVA 1000e-Series). The unit-cell parameters were obtained on refining the maxima of the XRD patterns with a least-squares refinement method using the CELREF program (Langmuir, J.; Bochu, B. Celref; http://www.inpg.fr/LMGP; Laboratoire des Materiaux et du Ge´nie Physique de l'Ecole Supe´rieure de Physique de Grenoble.). Current-voltage (I-V) measurements were performed using a solar simulator with output intensity AM1.5 (100 mW/cm^2).

3. Results

(1) Au- incorporated $In(OH)_3$ and In_2O_3 nanoparticles[10]: With $InCl_3$ and $HAuCl_4$ as precursors under basic conditions, $In(OH)_3$ and In_2O_3 nanomaterials incorporating elemental gold were synthesized by a hydrothermal process and thermal decomposition. Both Au-incorporating products appear violet-red (Figure 1a). XRD patterns of Au-incorporating $In(OH)_3$ and In_2O_3 samples match the diffraction features of not only $In(OH)_3$ and In_2O_3 but also metallic Au (Figure 1b).

The SEM image of the Au-$In(OH)_3$ sample shows nanocrystals of rectangular shape with edge length 20~60 nm. After complete decomposition at 450 °C, the $In(OH)_3$ nanocrystals of rectangular shape were fully transformed into In_2O_3 with no significant alteration of the overall morphology (Figure 2).

Transmission electron microscopy (TEM) for a $In(OH)_3$ single crystal exhibits rectangular shape and selected-area electron diffractions (SAED) exhibit [001] zone-axis diffraction of bcc $In(OH)_3$ (inset of Figure 3a), indicative of a single-crystalline

product. Figure 3b shows a TEM image from an Au-incorporating $In(OH)_3$ single crystal that is covered with a thin film of unknown material (thickness ~ 1 nm). The SAED pattern clearly shows a four-fold axis that can be indexed with hk0 of $In(OH)_3$, indicative of a single-crystalline $In(OH)_3$ nanocrystal. EDS measurements show the existence of Au, In and O elements. These results indicate that the $In(OH)_3$ nanocrystal is covered with a thin layer of elemental gold. An area scan of elemental Au on the surface of $In(OH)_3$ nanocrystals shows an uneven distribution of Au, indicating that the surface of the $In(OH)_3$ nanocrystal is incompletely covered by Au. Figure 3c is a TEM image of an In_2O_3 nanobundle of rectangular shape that exhibits a highly porous morphology formed by interconnected indium-oxide nanocrystals with average pore diameter 3-5 nm. The wall thickness is about 5 nm for most aggregated rectangular bundles. Selected-area electron diffraction (SAED) performed on an In_2O_3 bundle revealed a pattern of rings and dots that is indexed to cubic In_2O_3, indicative of the polycrystalline nature of the nanoporous In_2O_3 product. When Au is incorporated into this In_2O_3 nanoporous material, the shape of the Au-In_2O_3 bundle is essentially the same as the In_2O_3 product with small pores of diameter ~ 3 nm; this form is unprecedented for an indium-oxide nanostructure (Figure 3d). An EDS area scan for elemental Au show a scattered distribution of Au signal, indicating that the Au element was incorporated into the In_2O_3 rectangular bundle. The results indicate that the Au film in

$In(OH)_3$ melted during calcination to form small particles of Au, which diffused further into the nanoporous In_2O_3 bundle. The BET surface areas of Au-$In(OH)_3$ and Au-In_2O_3 are 26.2 and 35.5 m^2/g, respectively, comparable with a commercial nanoparticle sample of In_2O_3 for which the surface area is 27 m^2/g. The results are consistent with a porous structure according to the SEM/TEM measurements.

The UV diffuse reflection spectra of both Au-incorporating samples show clearly an intense absorption maximum about 532 nm, attributed to the surface-plasma excitation of gold nanoparticles (Figure 4a). The band gaps of $In(OH)_3$ and In_2O_3 host materials are calculated to be 5.57 and 3.74 eV, respectively, which are similar to reported values. Photoluminescence (PL) spectra of both In_2O_3 and Au-In_2O_3 nanoporous materials show a strong and broad PL emission in the blue-green region with its maximum intensity centered at 467 nm; this sharp blue-green emission is attributed to the radiative recombination of a photo-excited hole with an electron occupying oxygen vacancies in the In_2O_3 host, analogous to the PL mechanism of ZnO defect nanocrystals. During the thermal decomposition, oxygen vacancies are expected to be generated at a large concentration because of O and H bonds released and In_2O_3 crystallization. Similar PL spectra with maxima in the blue-green region are reported for In_2O_3 nanoparticles, nanocubes and nanofibers.

According to the experimental observations we propose a mechanism for the formation of the Au-incorporating

nanomaterials. As illustrated in Figure 4b, the $Au(OH)_4^-$ complexes were initially attached at the surface of $In(OH)_3$ colloids during the hydrothermal process. The Au^{3+} ions became subsequently reduced by chloride ion under basic conditions according to this reaction:

$$2\ Au(OH)_4^- + 3Cl^- + 2OH^- \rightarrow 2Au + 3ClO^- + 3H_2O$$

The reduced elemental Au covers the surface of $In(OH)_3$ nanocrystals. During thermal decomposition, the newly formed indium oxide begins to form on the surface of $In(OH)_3$. The O and H bonds of molecules were released within the $In(OH)_3$ nanocrystal and caused the formation of small voids or pores until indium hydroxide is completely decomposed to form nanoporous indium oxide. The Au film melted to form Au nanoparticles, which diffused into the pores or interstitial regions of In_2O_3 bundles.

(2) Synthesis ZnO nanorod film and Co^{2+} doped ZnO nanoparticles and nanorod: SEM image of ZnO nanorods on ITO film reveals average diameter and length of ZnO nanorod of ~50 and 100 nm, respectively (Figure 5a). The as-synthesized ZnO rod/ITO films were used as the metal oxide electrode to fabricate solar cell device. The photocurrent measurements of ITO film covered by ZnO nanorods reveals photo energy conversion efficient of 0.04 %, which is higher than the ITO film with ZnO nanoparticles (η = 0.018 %). The results indicate that the ZnO nanorod could enhance the solar cell activity. The study for the effect of size in ZnO rods to photo currents is in progress. The Co^{2+} doped ZnO

nanoparticles were synthesized with different wt% of Co^{2+} and the SEM images for Co-ZnO nanoparticles are shown in Figure 6a. The results indicate that the initial amount of Co^{2+} ion affect the shape of Co-ZnO nanocrystals that varied from needle shape (10, 20, 40 wt%) to rod shape (80 %)and finally to hexagonal rod shape crystals (120, 200%). UV-vis spectra shows band gap absorption at $\lambda \sim 400$ nm and ligand field absorption in the visible light region between 550 and 700 nm (Figure 6b). The intensity of ligand field absorption is increase as the Co^{2+} doping concentration is raised.

(3) The effect of InTe nanoparticles to photocurrent: The InTe nanoparticles were synthesized under different condition to study their effect to photocurrent (Table 1). Solar cell devices with films of InTe/TiO_2 were fabricated for photocurrent measurements (Figure 7). When small amount of InTe nanoparticles was introduced to the film, the photocurrent increased. The film with crystalline InTe nanoparticles exhibits the most pronounce photo energy conversion efficiency.

4. Conclusion

$In(OH)_3$ and In_2O_3 nanocrystals of rectangular shape and incorporating Au film and nanoparticles have been successfully prepared using a hydrothermal reaction followed by thermal decomposition. This procedure will be readily generalized to prepare other metal-incorporating nanoporous metal-oxide materials to serve as catalyst, gas sensor, and quantum-dot solar cell substrate. The Co^{2+} doped ZnO nanoparticles show strong absorption in visible light region and their particle shape and

thermodecomposition of Zn(tda)H_2O. The as-prepared ZnO coated ITO substrate was placed to a solution of zinc nitrate (5 mM, 98%, Riedel-de Haën) and hexamethylenetetramine (HMTA; 99%, Alfa-Aesar), follow by heating at T = 95 °C for 2 h.

(4) Synthesis of Co^{2+} doped ZnO nanoparticles: A solution of zinc nitrate (5 mM, 98%, Aldrich) and hexamethylenetetramine (HMTA; 99%, Aldrich) was prepared to mix with different amount of $Co(NO_3)_26H_2O$ (97.7%, Alfa-Aesar). The weight percentage of $Co(NO_3)_26H_2O$ was varied to 10, 20, 40, 80, 120, and 200 % compare to zinc nitrate. The reactions were carried out at T = 95 °C for 2 h.

(5) Synthesis of TiO_2 nanocrystals: Nanocrystalline TiO_2 in anatase form was synthesized via a combined sol–gel process with hydrothermal treatment. In typical synthesis, a specified amount of 2-propanol (10 ml) was first introduced into $Ti(OR)_4$ (37ml). The mixed solution was then gently added drop wise into a solution of water (250 ml) and acetic acid (80 ml) under N_2 flow. The solution became pale blue solution after the process was done. The mixture was continuously stirred at 80 °C for 3 hours to obtain white sol. Then, the gel was cooled to room temperature to become pale blue, transparent solution. Subsequently, the gel was dried at 80 °C 3 hrs, the dried sample was calcined at 500 – 700 °C for 1 – 24 h to produce the desired mesoporous TiO_2 photocatalyst. The spin coating method was used to prepare TiO_2 film.

Co^{2+} concentration is tunable. The deposition of crystalline InTe nanoparticles to TiO_2 film show enhancement of photocurrent.

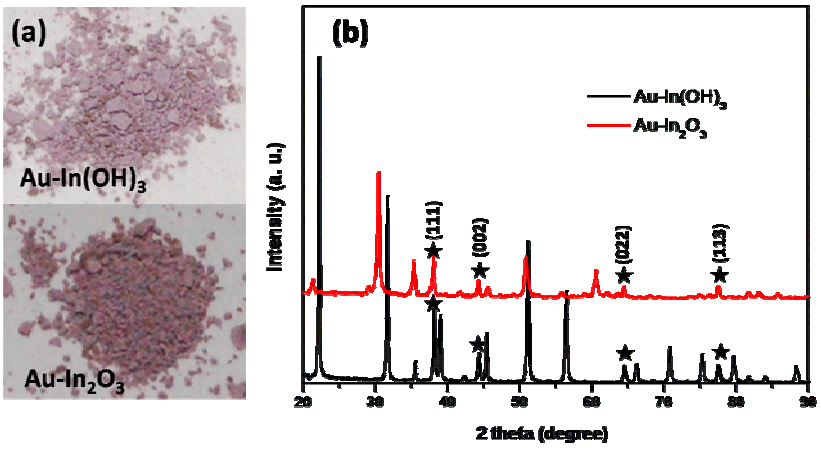

Figure 1. a) Appearance of Au-$In(OH)_3$ and Au-In_2O_3 powder samples, b)Powder x-ray diffraction patterns of Au-$In(OH)_3$ and Au-In_2O_3.

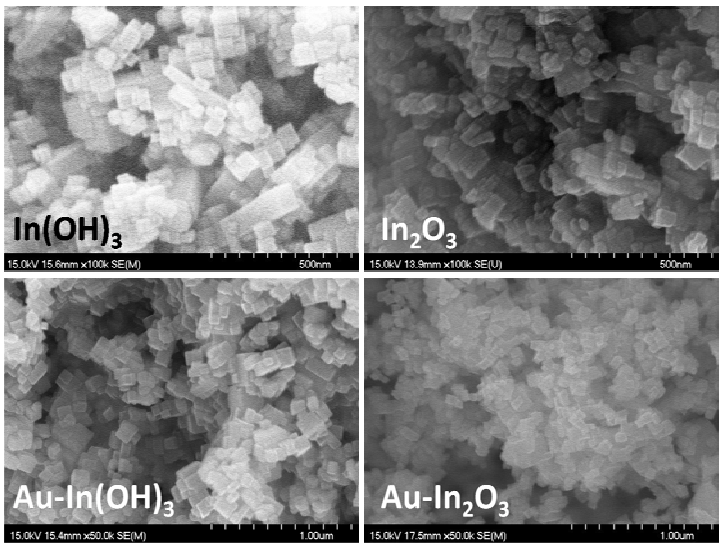

Figure 2. SEM images of $In(OH)_3$ and In_2O_3 and their corresponding Au-incorporated nanocrystals.

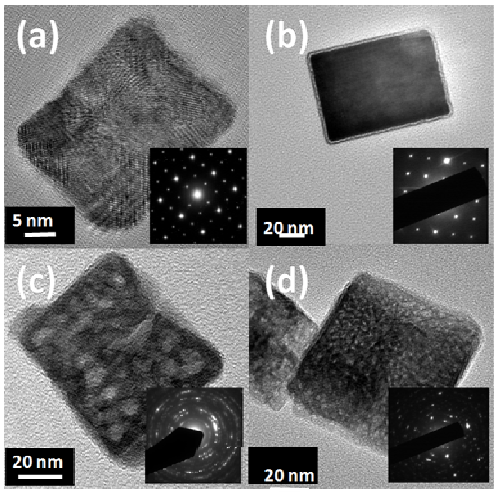

Figure 3. TEM images and corresponding SAED patterns (insets) of (a) $In(OH)_3$, (b) Au-$In(OH)_3$, (c) In_2O_3 and (d) Au-In_2O_3.

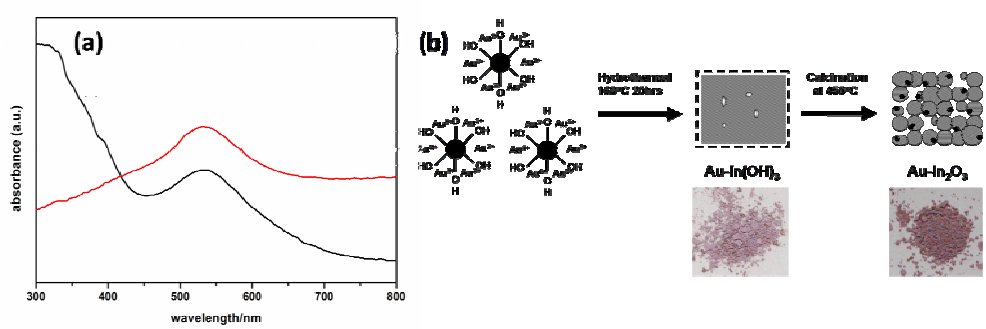

Figure 4. a) UV-vis diffuse reflectance spectra of Au-$In(OH)_3$ (black) and Au-In_2O_3 (red). b) A schematic illustration for the transformation of an Au-incorporating indium hydroxide rectangular nanocrystal to a nanoporous indium oxide rectangular nanobundle through hydrothermal and thermal decomposition.

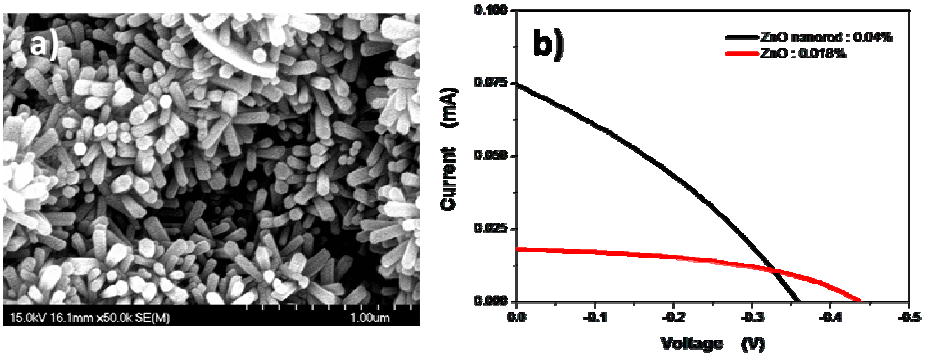

Figure 5. a) SEM image of an ITO film covered by ZnO nanorod. b) I–V curves of solar cells based on films of ZnO nanoparticle/ITO film (red) and ZnO nanorod/ITO film (black). The I_2/I^- solution was used as electrolytes; light intensity was 100 $mWcm^{-2}$ from an AM 1.5 source).

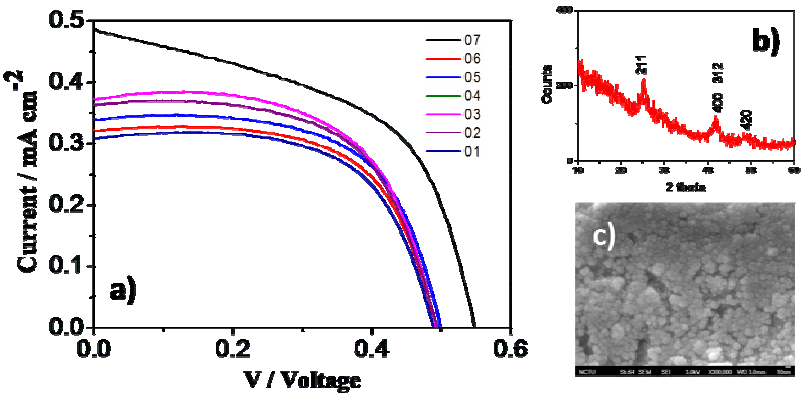

Figure 6. a) UV diffuse reflectance spectra for products of Co^{2+} doped ZnO nanoparticles. The labeled percentages of Co^{2+} are based on the experiment amount of $Co(NO_3)_26H_2O$ weight percentage. b) SEM images of Co^{2+} doped ZnO nanoparticle with different staring weight percentage of Co^{2+}.

Table 1. Summary of reaction conditions for InTe synthesis.

Rxn Conditions	Rxn. Time	Temp	Quench	η	V	I	F. F.
TiO_2 blank				0.114(0)	0.490(0)	0.48(2)	0.48(1)
InTe01	2min	180°C	N	0.096(0)	0.48(0)	0.31(0)	0.64(0)
InTe02	4min	180°C	N	0.095(1)	0.49(1)	0.32(0)	0.60(1)
InTe03	6min	180°C	N	0.112(1)	0.50(1)	0.37(0)	0.61(1)
InTe04	8min	180°C	N	0.104(6)	0.49(1)	0.35(1)	0.60(4)
InTe05	4min	200°C	N	0.106(1)	0.50(0)	0.34(0)	0.63(1)
InTe06	4min	180°C	Y	0.0998(1)	0.49(0)	0.32(0)	0.64(0)
InTe07	60min	180°C	N	0.134(5)	0.55(1)	0.48(1)	0.52(2)

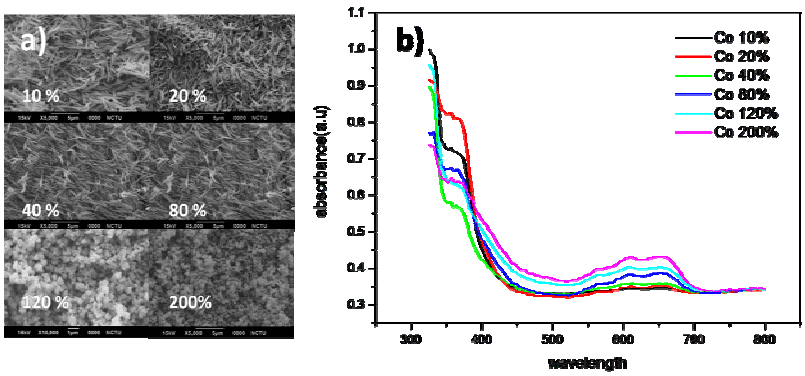

Figure 7. a) I–V curves of solar cell devices based on films of InTe nanoparticle/TiO_2 film with InTe nanoparticles from reaction InTe01-InTe07. b) Powder x-ray pattern of InTe sample from InTe07 reaction. b) SEM image of InTe/TiO_2 film.

References:

1. M.-C. Wu and C.-S. Lee, “Synthesis and Optical Properties of $M_xZn_{1-x}O$ Nanosponge (M = Mn, Fe, Co, Ni)” in Joint Symposium on Chemical Kinetics and Renewable Energy: from Gas phase to Condensed Phase, Hsinchu, Taiwan, 2007.
2. Y.-T. Zhang and C.-S. Lee, “Synthesis and Photovoltaic Measurement of Nanocrystalline In_2Te_3 Quantum Dots on TiO_2 film” in Joint Symposium on Chemical Kinetics and Renewable Energy: from Gas phase to Condensed Phase, Hsinchu, Taiwan, 2007.
3. M.-C. Wu and C.-S. Lee, “Synthesis and Characterization of Heterometallic Coordination Polymers $M'_xM''_{1-x}(tda)H_2O$ (M' and M'' =Zn, Co and Ni, $0<x<1$)” in The 8th Conference of the Asian Crystallographic Association, Taipei, Taiwan, 2007.
4. M.-C. Wu and C.-S. Lee, “Synthesis and Optical Properties of $M_xZn_{1-x}O$ Nanosponge (M = Mn, Fe, Co, Ni)” in The 8th Conference of the Asian Crystallographic Association, Taipei, Taiwan, 2007.
5. M.-C. Wu and C.-S. Lee, “Synthesis and Optical Properties of $M_xZn_{1-x}O$ Nanosponge (M = Mn, Fe, Co, Ni)” in 2nd Asia-Oceania Forum for Synchrotron Radiation Research, Hsinchu, Taiwan, 2007.
6. S.-Y. Chen, C.-S. Lee and M. C. Lin, “Metal and semiconductor nanoparticles application in solar cell” in Joint Symposium on Chemical Kinetics and Renewable Energy: from Gas phase to Condensed Phase, Hsinchu, Taiwan, 2007.

7. C. H. Lee, M. Kim, T. Kim, A. Kim, J. Paek, J. W. Lee, S.-Y. Choi, K. Kim, J.-B. Park and K. Lee, In_2O_3 cube. J. Am. Chem. Soc. 2006, 128, (31), 9326-9327.
8. Z. Zhuang, Q. Peng, J. Liu, X. Wang and Y. Li, $In(OH)_3$, InOOH, In_2O_3 nanocube-2007 $In(OH)_3$ InOOH In_2O_3.pdf. Inorg. Chem. 2007**,** 46, 5179-5187.
9. Y. C. Chang and L. J. Chen, ZnO rod, film. J. Phys. Chem. C 2007**,** 111, 1268-1272.
10. S.-Y. Chen, C.-S. Lee and M. C. Lin, Synthesis of $In(OH)_3$ and In_2O_3 Nanomaterials Incorporating Au. Inorg. Chem. 2007**,** Submitted.

二、Characterization of semiconductor nanoparticles (K. W. Sun):

1. Research methods and processes

(1) Visible light absorption and Photoluminescence from Co doped ZnO nanorods**:** The co-doped ZnO nanorods with different Co compositions are prepared by Prof. C.S. Lee's research group. The nanorod under investigation has an average length of 1 μm and a diameter of 200~300 nm. The Co dopants can introduce impurity levels in the ZnO bandgap to enhance absorption of the ZnO in the visible light wavelength range. The micro-PL from the impurity levels are studied by excited the ZnO $(Co)_x$ with a DPSS laser operated at wavelength of 488 nm. The emission is recorded through a confocal microscope equipped with a 0.32m spectrometer and a liquid-nitrogen cooled CCD.

(2) Nano PN junction for Si solar cell: Through E-Beam lithography and epi-layer growth techniques, we have fabricated PN diodes with nano meter scale junctions. The I-V characteristics of the diodes with nano junction are measured with a probe station. The reduced junction cross-section can reduced the dark current (thermal generation current in the diode depletion regions) by an order of magnitude. The reduction of dark current can lead to the increase of Si solar cell conversion efficiency and detectivity of Si photodiode.

(3) Charge transport in the TiO_2 film: We have devised a time-of-flight measurement system to investigate the photocurrent transient in TiO_2 solar cells. We compare the results between TiO_2 solar cells prepared with different solvents. The faster decay of photocurrent indeed reflects on the better conversion efficiency of the solar cell.

2. Main discoveries and conclusions

(1) Visible light absorption and Photoluminescence from Co doped ZnO nanorods**:** A broad absorption peak from 550 nm to 680 nm is observed in the absorption spectrum of the $ZnO(Co)_x$, as shown in Figure 1. Figure 2 to 4 show the emission peaks at visible wavelengths from 566 nm to 684 nm. The emission peaks are resulted from the doped Co impurity levels in the mid-gap of ZnO.

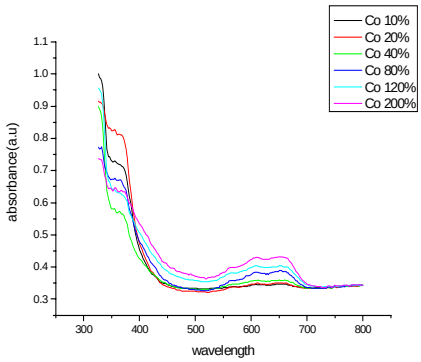

Figure 1

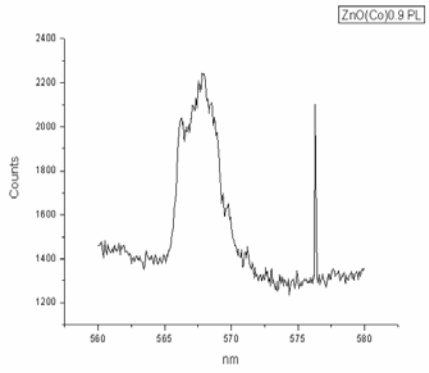

Figure 2

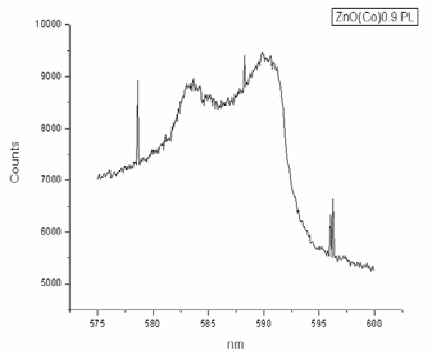

Figure 3

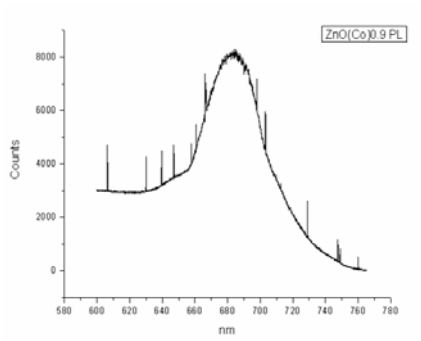

Figure 4

(2) Nano PN junction for Si solar cell: An Oxide layer of thickness of 100 nm is first grown on a 4 inch Si wafer after the RCA cleaning processes. The nanostructured templates were prepared using electron-beam (e-beam) lithography techniques on Si (001) substrates. The flow chart of the lithography and etching processes is given in Figure 5. Nanopore patterns were directly written in a square area of about 200 μm x 200 μm with an electron - beam writer operated at a fixed electron voltage of ~ 50 KV. By using the patterned ZEP-520 as the hard mask, the exposed Si area was then etched into the substrate with a depth of approximately 120 nm below the Si surface via the chemical wet etching processes. In Figure 6 we show the SEM images of the nanopores on one the templates we made.

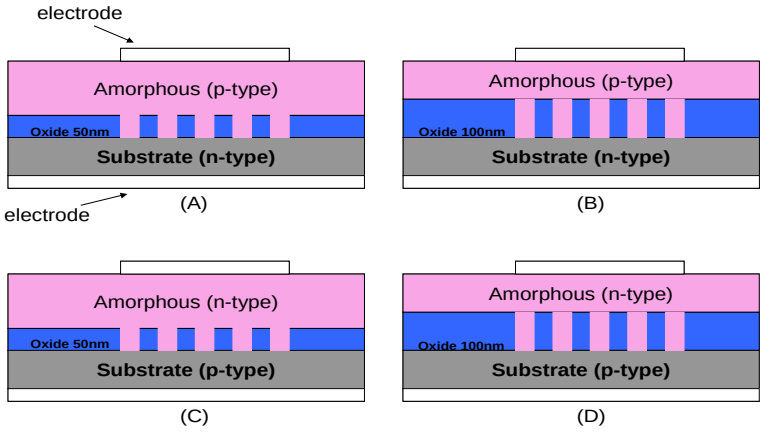

Figure 5

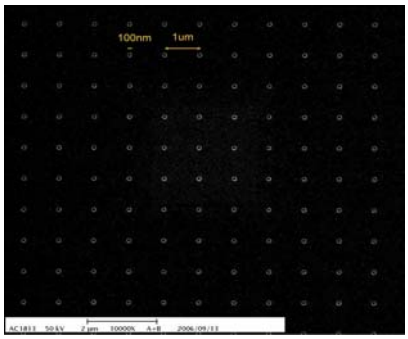

Figure 6

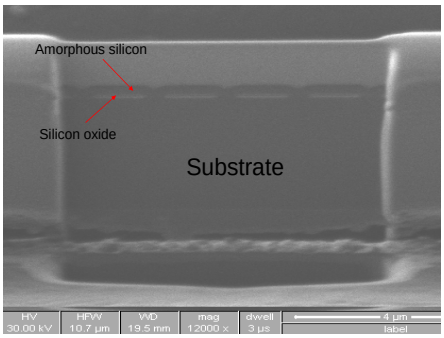

Figure 7

A layer of p-type amorphous silicon is grown on the nanostructured template by via PECVD to form the nano PN junction. The TEM image of the junction cross section is shown in Figure 7. The results of the I-V measurement of the device is shown in Figure 8.

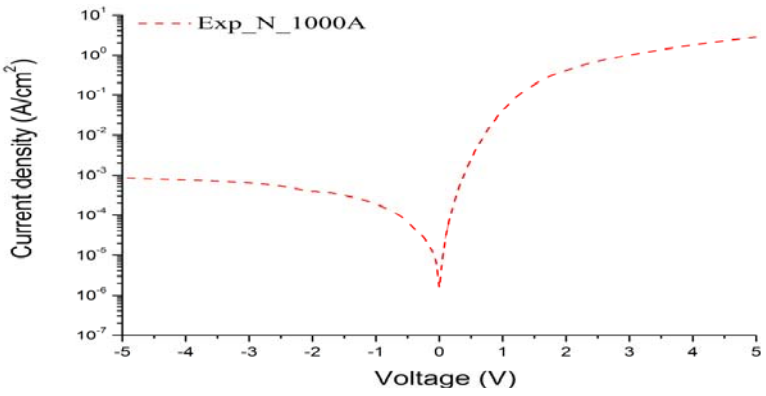

Figure 8

(3) Charge transport in the TiO_2 film: Two TiO_2 solar cells made from P25 powder are prepared with the solvents of HNO_3 and Acetic acid. The I-V characteristics of the two solar cells are shown in Figure 9. The solar cell prepared with the HNO_3 solvent gives a better performance on the conversion efficiency over the cells prepared with the Acetic acid. In Figure 10, the time-of-flight measurements also show shorter photocurrent decay time for the cells using HNO_3 solvent. It indicates that it is much easier for the electrons to transport in the TiO_2 film prepared with HNO_3 solvent.

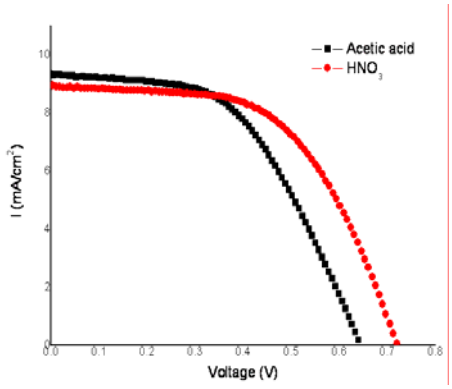

Figure 6

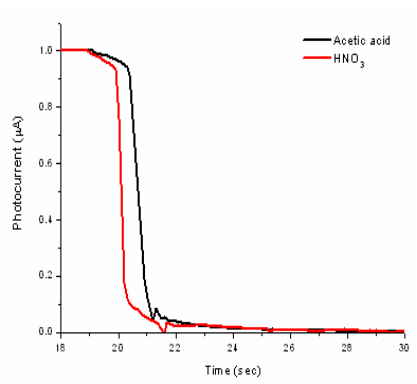

Figure 7

References:

1. S. C. Lyu, Y. Zhang, H. Ruh, H.-J. Lee, H.-W. Shim, E.-K. Suh and C. J. Lee, "Low temperature growth and photoluminescence of well-aligned zinc oxide nanowires", Chemical Physics Letters, 2002, 363, 134-138
2. C. Yang, C. J. Barrelet, F. Capasso, et al. Nano Letters, 2006, 6, 2929-2934
3. B. van der Zanden, A. J. Goossens, J. Phys. Chem. B, 2000, 104, 7171

4. A. C. Fisher, L. M. Peter, E. A. Ponomarev, A. B. Walker, K. U. Wijayantha, J. Phys. Chem. B, 2000, 104, 949

三、InN/TiO_2 solar cells by PECVD and OMCVD:

1. InN/TiO_2 nanoparticles by PECVD (C. W. Lu, Y. P. Lee and M. C. Lin)

   TiO_2 nanoparticles were prepared according to a method similar to that reported by Zaban and coworkers.[1] The sol-gel solution with a TiO_2 nanoparticle colloid was synthesized via a controlled hydrolysis of titanium (IV) isopropoxide, $Ti(i\text{-}OC_3H_7)_4$ (Aldrich, 97 %) in an aqueous solution of glacial acetic acid at 273 K. The solution was then heated to 353 K for 8 h before being autoclaved at 503 K for 12 h. The resulting TiO_2 sol-gel solution was spread onto a clean Ti foil or a conducting glass substrate (FTO, F-doped SnO_2, sheet resistance 10 Ω cm^{-2}) and baked in an oven at 723 K for 1 h to form TiO_2 films with nanoparticles of typical sizes 20–30 nm. TiO_2 nanoparticles of big sizes could be prepared on increasing the autoclaved temperature.

   Figure 1 is a schematic diagram of the experiment for PECVD. The reactor is a quartz tube (diameter 5 cm) with a sidearm (diameter 0.6 cm, length 5 cm) for pressure measurements; the reactor is evacuated with an oil mechanical pump. A controller (Omega, CN9000) regulated the reaction temperature through resistive heating of the reactor. InN nanoparticles were directly grown over TiO_2 nanoparticle films in the reactor using TMIn and NH_3. TMIn (Strem, > 98 % purity) was transferred to a stainless-steel tube after vacuum distillation; it was introduced to

the reactor with a small flow of He (99.9995 %) carrier gas via a stainless-steel ring (diameter 3 mm) perforated with small holes to provide a homogeneous flow onto the substrate. The distance between the TiO_2 film and the TMIn outlet is adjustable and was typically set at ~1 cm. The flow rate of TMIn was adjusted with a needle valve. A flowing gas mixture of NH_3 in He, subjected to microwave discharge (800 W), was introduced upstream of the gas flow to the reactor and served as the source of nitrogen. Flow rates of NH_3 and He were controlled with mass-flow controllers (MKS, model 1179 MFC) that were calibrated before and after experiments with a wet-test meter and, for smaller flows, through the pressure increase in a calibrated volume.

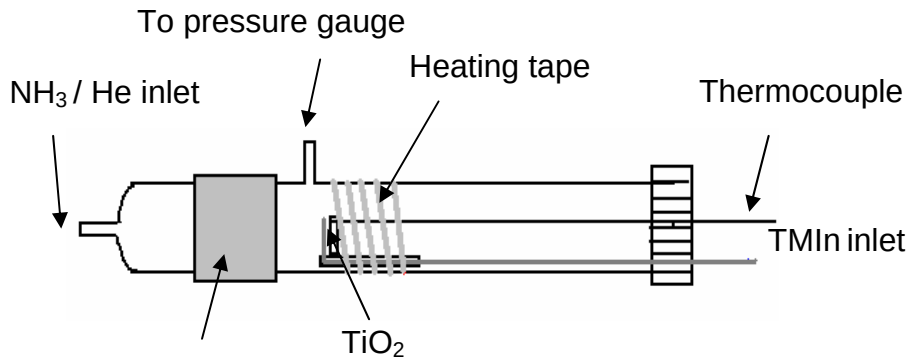

Figure 1: Schematic diagram of the experimental system for plasma-enhanced chemical vapor deposition (PECVD).

Before deposition of InN, the TiO_2 film was cleaned with an oxygen plasma at 523 K for 30 min. Typical experimental conditions were: total flow rate F_T = 60 STP cm^3 s^{-1} (STP denotes 1 atm and 273 K), flow rate of TMIn (820 ppm in He) F_{TMIn} = 2–10 STP cm^3 s^{-1}, flow rate of NH_3 F_{NH3} = 20 STP cm^3 s^{-1}, total pressure P = 5.2 Torr, reaction temperature T = 358–623 K, duration of deposition t = 15–120 min.

Absorption spectra were recorded with a spectrophotometer (Jasco, model V–570). For photosensitization tests, the devices were assembled in a sandwich configuration with the TiO_2 film facing a Pt counter electrode, prepared on electron-beam deposition of a layer of Pt (thickness 200 nm) onto a FTO conducting glass. A film (Parafilm, 5×10 mm^2), on the periphery of the edge of the cell and placed between the Pt electrode and the TiO_2 film, served as a spacer for the electrolyte, producing an active area ~0.5 cm^2. The redox electrolyte solution comprised I_2 (0.3 M) and LiI (0.03 M) in propylene carbonate.

The solar cell was illuminated with a commercial solar simulator (Yamashita-Denso, model YSS–50A); its light intensity (or radiant power) was adjusted with a Si solar cell to simulate AM 1.5 solar radiation. Current–voltage (*J–V*) measurements were undertaken using a digital meter (Keithley, model 2440). The incident photocurrent conversion efficiency (IPCE) measurements were measured with a monochromator (Dongwoo Optron, model DM150i). A digital multimeter (Keithley, model 2400) was used to measure the photocurrent response from the sample.

Results and Discussions

InN on TiO_2 nanoparticles: Figure 2 shows a comparison of UV–vis spectra of TiO_2 and InN/TiO_2 films with various periods of deposition. Major absorption by a pure TiO_2 film occurs from 390 nm into the UV region. The spectra of InN/TiO_2 films show a pronounced broad absorption in the UV–vis range; the

absorption shifts to the red as the duration of deposition increases. The InN/TiO_2 film after deposition for 120 min shows significant absorption in the range 390–900 nm, similar to Grätzel's black dye.[2] This result indicates InN to be a suitable absorber of sunlight, confirming the observation recently made by Wang and Lin.[2]

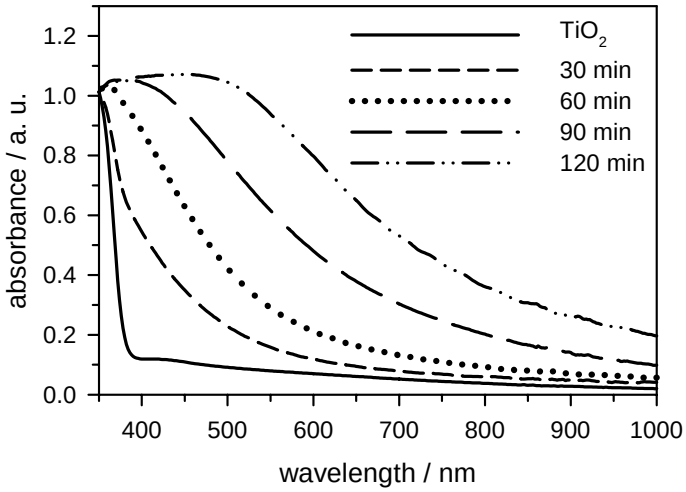

Figure 2. UV–vis spectra of a TiO_2 film (solid line) and InN/TiO_2 films with various durations of deposition. The spectrum is normalized at 350 nm. Deposition temperature 358 K; total pressure 5.2 Torr; flow rate of TMIn (820 ppm in He) = 6 sccm; flow rate of NH_3 = 20 sccm; duration of deposition: 30 min (short dashed line), 60 min (dotted line), 90 min (long dashed line), 120 min (dashed-dotted-dotted line).

We examined systematically the dependence of the photoelectrical behavior of InN-sensitized TiO_2 films on deposition conditions by varying separately the flow rate of the reagents, the temperature of the substrate, and the duration of deposition. The devices for analysis were illuminated with AM

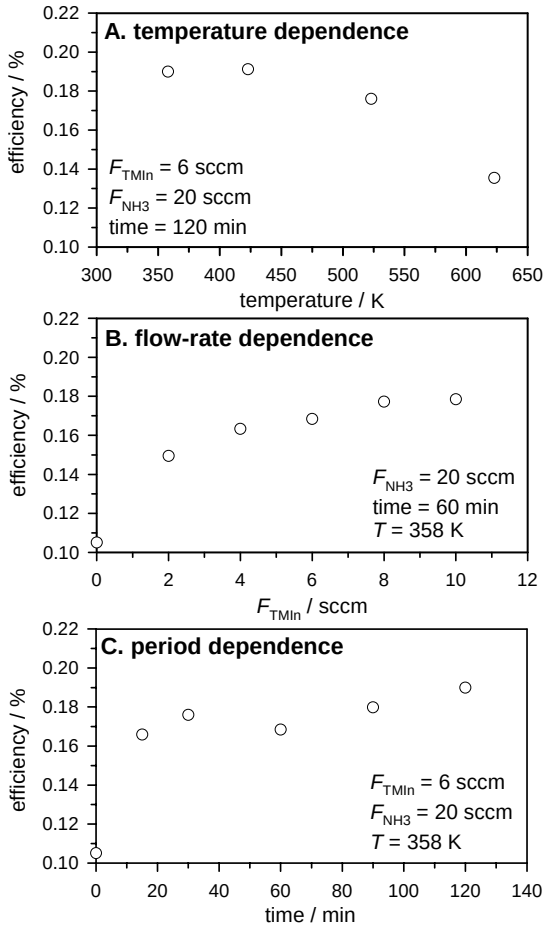

Figure 3. Dependence of efficiency (η) of power conversion on (A) substrate temperature, (B) flow rate of TMIn (820 ppm in He), and (C) duration of deposition.

1.5 solar radiation at 100 mW cm^{-2}. Figure 3 indicates the relations between the efficiency (η) of power conversion and deposition conditions. This efficiency, ranging ~0.14–0.20 %, generally increases with the size of InN particles; it thus increases as the deposition temperature is decreased, as the flow rate of TMIn is increased, or as the duration of deposition is increased. These trends approach a limit within a small range of experimental conditions, as shown in Figure 3. Based on this result, the best temperature for InN deposition of the TiO_2

substrate is below 423 K. Figure 4 shows SEM images of a side view of the InN/TiO_2 films. It is clear that only the surface layer of TiO_2 was coated with InN, the inner layer of TiO_2 film was uncoated. It appears that, in the PECVD process, the holes between TiO_2 nanoparticles on the surface layer were filled readily with InN and blocked the deposition of the inner layers, especially at a higher concentration or greater flow rates of TMIn. Under such conditions, the inner layer of TiO_2 film was not coated with InN; the efficiency therefore rapidly approached a limit at which the surface TiO_2 was coated with InN and a greater flow rate of TMIn or a greater duration of deposition provide no further contribution to the sensitization.

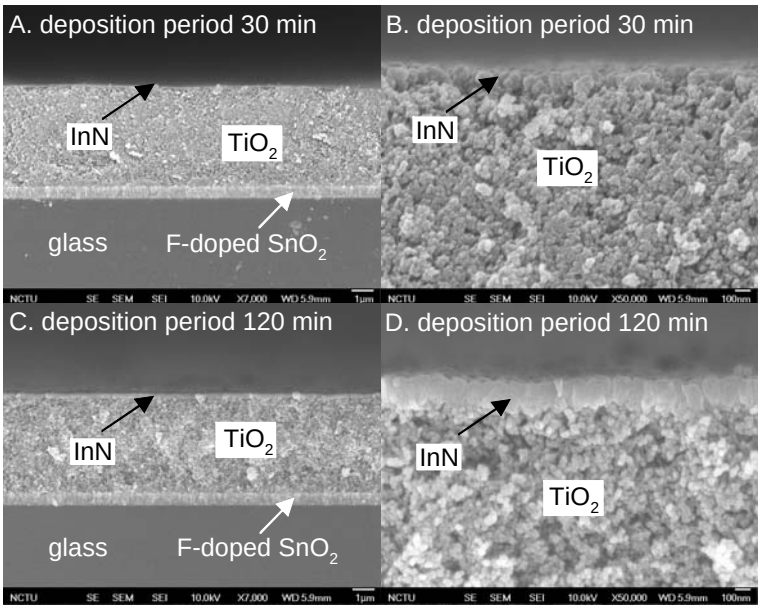

Figure 4. SEM images of a side view of InN/TiO_2 films. Deposition temperature 358 K; total pressure 5.2 Torr; flow rate of TMIn (820 ppm in He) = 6 sccm; flow rate of NH_3 = 20 sccm. (A) deposition period 30 min, ×7000; (B) same as (A) but with ×50000; (C) deposition period 120 min, ×7000; (D) same as (C) but with ×50000.

We also examined carefully the dependence of the photoelectrical behavior of InN-sensitized TiO_2 films on the thickness of the TiO_2 film. The open-circuit voltage is independent of the TiO_2 film thickness, and the short-circuit current increases by about 25 % as the thickness of the TiO_2 film increases from 0.7 to 5.9 μm; the thickness of the deposited InN was found to be ~330 nm in these experiments. These results indicate that TiO_2 has some contribution to the conversion efficiency and decreasing the thickness of uncoated TiO_2 does not increase the conversion efficiency, suggesting that charge recombination in the uncoated TiO_2 layer might not be the major factor limiting the efficiency of the film under present conditions.

Figure 5 presents a typical IPCE spectrum of TiO_2 and InN/TiO_2 films. All three InN/TiO_2 films show photocurrent responses below 550 nm in contrast with the TiO_2 film that responds only in the UV range ($\lambda < 390$ nm). Furthermore, with increasing period of deposition, the IPCE values of InN/TiO_2 films at longer wavelengths increase. This phenomenon is consistent with that indicated in the UV–vis absorption spectrum, but the IPCE decays rapidly as the irradiation wavelength increases. A large fraction of carriers are perhaps lost to charge recombination within the particle or at the InN/TiO_2 interface. Further improvement on the interface between InN and TiO_2 is needed in order to increase the efficiency of power conversion.

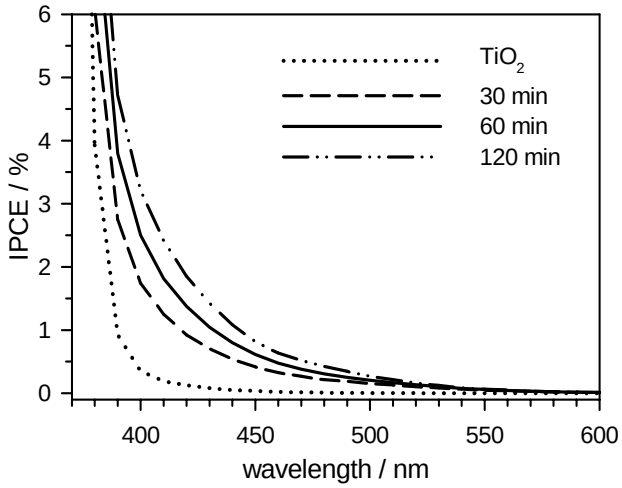

Figure 5. IPCE spectrum of a TiO_2 film (dotted line) and InN/TiO_2 films with various durations of deposition. Deposition temperature 358 K; total pressure 5.2 Torr; flow rate of TMIn (820 ppm in He) = 6 sccm; flow rate of NH_3 = 20 sccm. Deposition periods: 30 min (dashed line), 60 min (solid line), and 120 min (dashed-dotted-dotted line).

Figure 6 indicates the current–voltage (*J*–*V*) character of a reference TiO_2 film and our most efficient InN-sensitized TiO_2 sample. The measurements under simulated AM 1.5 sunlight illumination at 100 mW cm^{-2} indicate an open-circuit voltage V_{OC} = 611 mV and a short-circuit current J_{SC} = 0.688 mA cm^{-2}, with an efficiency ~0.24 % of power conversion and a filling factor *ff* = 0.58. A reference sample of uncoated TiO_2 indicates that the photocurrent density generated is much smaller than that of samples sensitized with InN nanoparticles, consistent with InN nanoparticles being efficient sensitizers for nanocrystalline solar cells based on TiO_2. The sample was irradiated under AM 1.5 solar illumination at 100 mW cm^{-2} for 5 h with no apparent decrease in its performance, indicating the robustness of this inorganic sensitizer.[3] Comparing with the

parameters (V_{OC} = 350 mV, J_{SC} = 1.8 mA cm^{-2}, *ff* = 0.48, efficiency = 0.3 %) of an InAs-sensitized TiO_2 nanocrystalline solar cell fabricated by Nozik and coworkers as alluded to in the Introduction,[3] our InN-sensitized TiO_2 solar cell has comparable values of V_{OC} and *ff*, with a somewhat smaller J_{SC}. This condition indicates that we must improve the contacts to the electrodes and the efficiency of electron transfer, and suppress the charge recombination to improve the conversion efficiency. Optimization of the particle surface, the amount of TiO_2 coated with InN and the electrolyte recipe,[4] and finding a good linker between InN and TiO_2 are expected to increase further the efficiency.

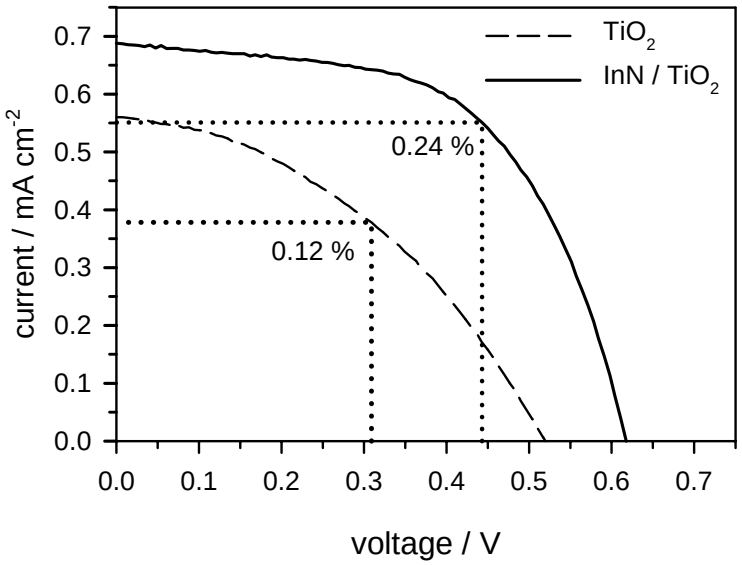

Figure 6. *J-V* characteristics of a TiO_2 film (dashed line) and an InN/TiO_2 film (solid line) under AM 1.5 illumination at 100 mW cm^{-2}. The photovoltaic parameters are V_{OC} = 611 mV, J_{SC} = 0.688 mA cm^{-2}, *ff* = 0.58, and power conversion efficiency = 0.24 %. Deposition temperature 358 K; total pressure 5.2 Torr; flow rate of TMIn (820 ppm in He) = 8 sccm; flow rate of NH_3 = 20 sccm; duration of deposition=2 h.

Conclusions

InN has been deposited onto a porous nanocrystalline TiO_2 substrate by means of plasma-enhanced chemical vapor deposition using trimethyl indium and ammonia as sources of indium and nitrogen, respectively. The sensitized InN/TiO_2 solar cell exhibits a performance similar to that reported for a nanocrystalline TiO_2 solar cell sensitized with InAs quantum dots; the photovoltaic parameters are V_{OC} = 611 mV, J_{SC} = 0.688 mA cm^{-2}, *ff* = 0.58 and efficiency = 0.24 % of power conversion, determined using an AM 1.5 solar simulator at 100 mW cm^{-2}. The performance of the solar cell may be improved with further modification and optimization. With an improved efficiency, the robust physical-chemical properties of the InN/TiO_2 system may afford the possibility of providing a low-cost photo-electrode for applications in solar energy conversion or water splitting.

References:

1. A. Zaban, S. Ferrere, J. Sprague and B. A. Gregg, J. Phys. Chem. B, 1997, 101, 55.
2. J.-H. Wang and M. C. Lin, ChemPhysChem, 2004, 5, 1615.
3. P. Yu, K. Zhu, A. G. Norman, S. Ferrere, A. J. Frank and A. J. Nozik, J. Phys. Chem. B, 2006, 110, 25451.
4. H. Nusbaumer, S. M. Zakeeruddin, J. Moser and M. Grätel, Chem. Eur. J. 2003, 9, 3756.

2. InN/TiO_2 nanoparticles by OMCVD (T. T. Wang and M. C. Lin):

TiO_2 sol gel was obtained from the acid-type reaction of i-Propanol and titanium isopropoxide developed by INER. Size well controlled to 20 nm TiO_2 nanoparticles were formed by 12hr 503K autoclaving and kept in hood to avoid light exposure before use. We first prepared the anti-reflection layer by spin coating TiO_2 sol-gel over conducting glass (FTO, fluorine-doped SnO_2) which may reduce the incident light loss during direct illumination. Layered anatase TiO_2 was screen-printed over anti-reflection layer in thickness of 2μm after 30 min baking at 723 K. After that the TiO_2 substrates were immersed in 0.1M $TiCl_4$ (aq) at 343K for 30 min to improve the "bridging" between separated nanoparticles. Finally, this bridging was solidified after 2 min 500 W microwave treatment, spinel shapes TiO_2 (Figure 7(A)) were formed between ordinary round nanoparticles. This modified buffer layer may improve the electron transfer efficiency greatly.

Among the InN deposition studies, the most efficient precursor of In was trimethyl-indium ($(CH_3)_3In$) which was purchased from Aldrich without any purification before use. The most used N source was hydrogen azide (HN_3) which was synthesized from reaction of sodium azide and phosphoric acid. The HN_3 product was purified by freeze-pump-thaw cycle under a hood to remove water and kept in an ethanol-dry ice mixture bath with extremely caution before use.

The deposition of InN was made with a homemade OMCVD system, The vacuum chamber was evacuated to lower than $2x10^{-7}$

torr and baked to 383 K before deposition taking place. During deposition, TiO_2 substrate was heated by thermal radiation from tungsten wire to a desired temperature. Then TMIn and HN_3 were introduced into the vacuum chamber simultaneously. The pressure of the reactant was HN_3: TMIn=$1x10^{-5}$:$2x10^{-6}$ tore. The TMIn/HN_3 ratio was kept at 1/5. After deposition time (2-120 min), the substrates were annealed at 723 K to reduce crystalline defects.

Fabrication of our InN/TiO_2/FTO solar cell is similar to the TiO_2 based DSSC. The devices were assembled in a sandwich configuration with InN/TiO_2/FTO photoanode facing a counter Pt electrode. The semi-opaque counter Pt electrode was made by using e-gun to vaporize Pt and condense the Pt particles on ITO glass with thickness as 20 μm. An enclosed spacer filled with I^-/I_3^- electrolyte with volume ~8 mm^3 was insert between Pt and TiO_2 electrode. The electrolyte was 0.3M 1,2-Dimethyl-3-propylimidazolium iodide, 0.03M I_2 and 0.5M t-butyl pyridine in 3-methoxypropionitrile.

To measure solar cell efficiency, we set up an YSS-50A AM1.5 solar simulator which has a good solar spectral output and light intensity stability at 100 mW/cm^2 solar radiation. The Keithley sourcemeter 2440 was used in J-V curve measurement. Light intensity was calibrated by using Gentec SOLO PE power meter coupled with UP19K-15S-H5 Si photodetector head. For our rugged surface substrates, we take the absorption spectra in the Integrating Spheres to avoid the undesirable diffraction interference.

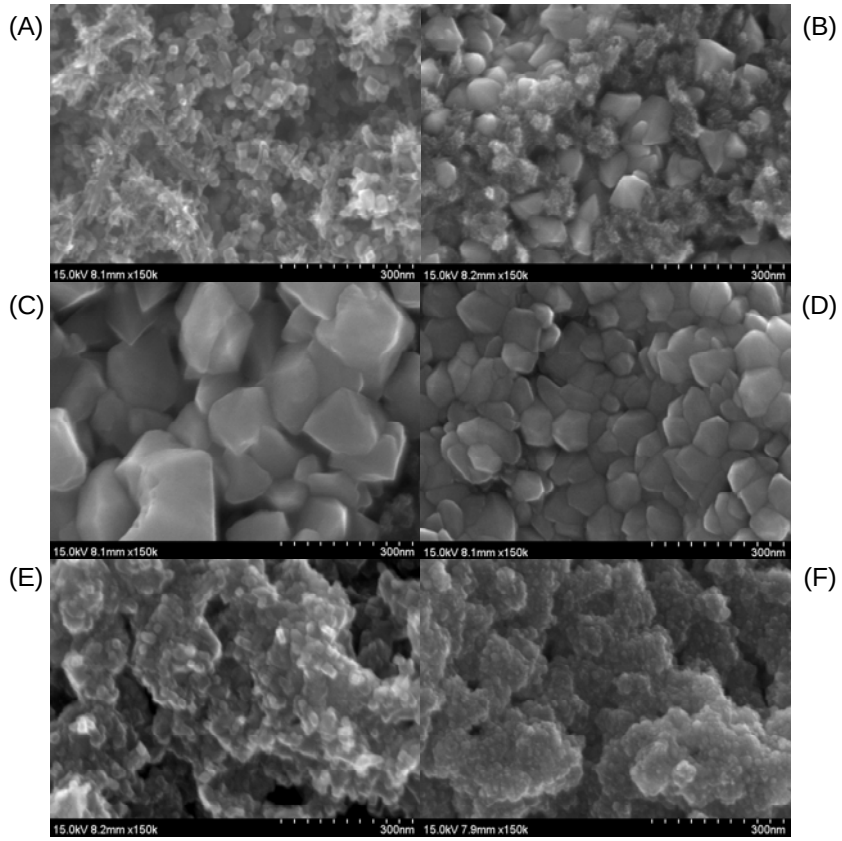

Figure 7. SEM images of InN/TiO_2 (A) $Ti(OH)_4$ modified TiO_2; InN deposit on the TiO_2 surface at 723 K after (B)20min and (C)2hr deposition time. 2hr deposition at different temperature (E) 673 K, (F) 623 K, (G) 583 K.

Results and Discussion:

In Figure 7, we present the high resolution SEM morphologies of (A) modified 15-20nm TiO_2 nanoparticles, grown InN on TiO_2 after (B) short time and (C) ~ (F) long time deposition. After 2hr deposition in our low pressure OMCVD system, significant InN particles were observed and no indium droplets formed on the surface for operating temperature above 583 K. The averaged InN particle size is estimated to be 15, 30, 90 and 150 nm at operation temperature of 583, 623, 673 and 723 K, respectively. It is clear to see that InN wraps up $Ti(OH)_4$-modified spinel

shape TiO_2 nanoparticles, and ball-like corpuscles are formed at T< 623 K deposition in contrast to the giant particle grown "above" TiO_2 surface at high temperature. The loose contact between InN and TiO_2 for the high temperature sample implies the electron transfer is unfavored in optoelectronics applications.

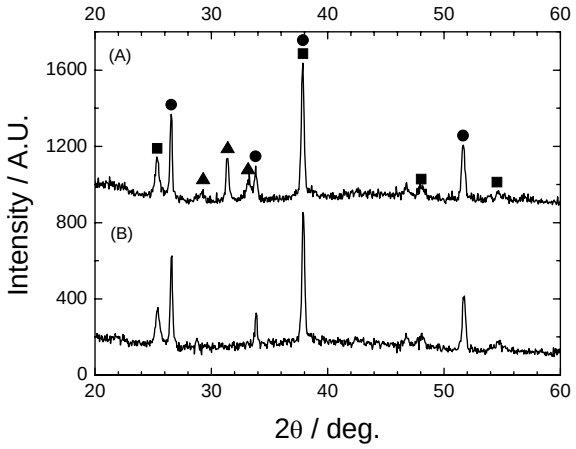

Figure 8. XRD spectrum of InN/TiO_2/FTO after 2hr CVD deposition at (A) 673 K (B) 533 K. (■Anatase TiO_2●SnO_2▲InN)

In Figure 8 X-ray diffraction studies, three group peaks are observed including: anatase TiO_2, SnO_2 for FTO conducting glass and InN particles. In contrast to the low deposition temperature sample which lacks crystallinity, several orientations (100), (002) and (101) of InN are observed for the samples above 673 K reveal that polycrystalline InN is deposited on anatase TiO_2. Amorphous sample can be re-crystallized and morphologies are greatly improved by annealing at 723 K. The deposited InN posseses two strongest peaks of (002) and (101) which are also the most observed orientations of the InN films on different substrates in previous OMCVD experiments. The stoichiomertric ratio was examined by EDX analysis (see Table

1), indium to nitrogen ratio was kept steadily around 0.7 at T>623K, indicating nitrogen rich-films.

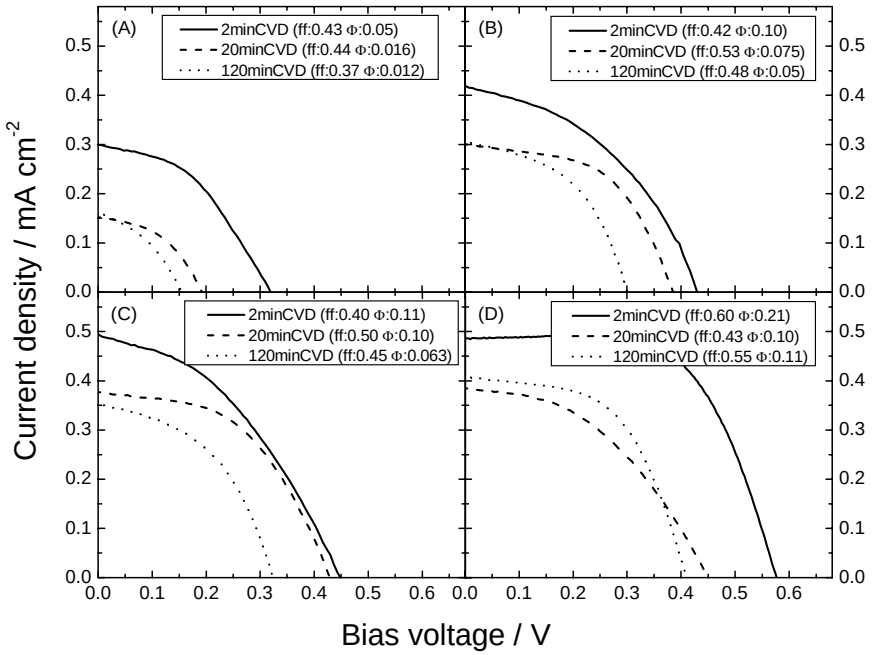

Figure 9. Quantum efficiency of InN/TiO_2 system at different temperature (A) 723K (B) 673K (C) 623K (D) 583K with deposition time of 2min (solid) 20min (dash) and 120min (dot).

Figure 9 shows systematic analysis of J-V diagram at different temperature by varying deposition time from 2 to 120 min with incident light as 100 mW/cm^2 and exposure area of 0.4 cm^2. It is clear to see that both the J_{sc} and V_{oc} drop a lot at higher deposition temperature and longer deposition time. Energy lost with grown crystalline defects could explain the short time deposition sample which posseses the highest conversion efficiency at any given temperature. For the high temperature CVD sample, electron transfer is limited due to loose contact between InN and TiO_2 which is reflected by its poor efficiency. Among all, the best quantum efficiency obtained is about 0.21%

after 2 min deposition at 583K. To further study the electron transfer process in our InN/TiO_2/FTO system, we reduce the incident light intensity by placing a neutral density filter which has a flat spectral response curve from 250 nm~2000 nm. The attenuated light intensity is carefully calibrated by a Si photodetector. We found that the photo-current efficiency increased from 0.21% to 0.35 and 0.41% when the incident intensity were reduced to 20 and 9mW cm^{-2} (Figure 4), respectively. With a little bit drop in V_{oc} (from 0.575 to 0.55V), the photocurrent intensity increase twice while the incident light reduces to 1/10 of the one sun-condition. This phenomenon had been discussed among the studies employing cobalt complexes as redox couple relays in DSSC and InAs QDSSC and Na_2S as electrolyte in CdSe QDSSC. The limiting factors of current decrease under high incident light intensity may be: (i) mass transport limitation of redox pair and (ii) the enhancement of charge recombination of electron in TiO_2 and holes in QDs for QDs type solar cell. The limitation of redox pair might be overwhelmed by using a higher concentration electrolyte. However, in our study, in comparison of J-V curve obtained with 0.01M and 0.005M iodine concentration in electrolyte, both show that fill factor increases from 0.6 to 0.77 under lower incident light intensity, which means the alternation in redox couples is no longer the limiting factor. Thus, the decreasing photocurrent might be due to that: the electron transport is restricted by enhancement of back-charge- recombination of electron and hole pair under a high incident light.

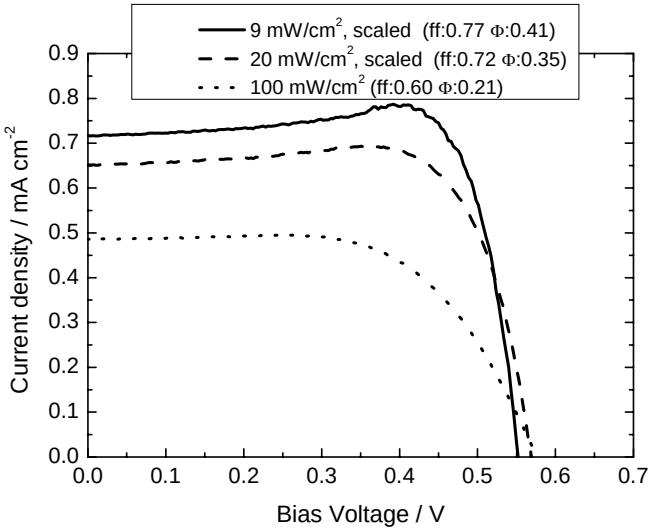

Figure 10. Quantum efficiency of InN/TiO_2 system at different incident intensity 100(dot), 20(dash) and 9mW/cm^2 (solid).

Table 1. EDX analysis of atomic ratio of InN/TiO_2/FTO substrate.

%	723 K	673 K	623 K	583 K	433 K
N /K	13.03	22.27	12.55	1.48	-
O /K	45.73	25.38	47.86	61.90	70.52
Ti /K	32.03	37.56	30.13	31.79	27.95
In /L	9.21	14.79	9.46	4.83	1.33
In/N ratio	0.71	0.66	0.75	3.26	-

For the DSSC or QDSSC, the absorbing molecules were chemisorbed by immersing TiO_2 substrate in "absorber" dye molecules or QDs solution. Thus, a highly porous structure and multi-layered nanocrystalline TiO_2 film will improve the photo efficiency by accommodating more absorbers. The grown InN nanoparticles showed better adhesion on TiO_2 surface than the weak chemical adsorption of absorbers. And InN/TiO_2/FTO system shows a great stability in conversion efficiency by reassembling the departed device tested weeks ago. However, the

direct deposition restricts InN particles in the very superficial layer of TiO_2. Thus the total efficiency is rather limited to date. To overcome this drawback, alternative InN growth methods are carried out in our group.

Conclusion:

In this work, we studied InN deposition on anatase TiO_2 nanoparticles at different temperatures by the reaction of TMIn and HN_3 using low pressure OMCVD. The averaged InN particles sizes are ranging from 15 to 20 nm for depositions at different temperatures. After annealing at 723 K, crystallized InN can only be grown by T > 583 K deposition. In the AM1.5 measurement, among all the devices, photo-efficiency 0.41% had been achieved under low intensity 9 mw/cm^2 illumination. The efficiency decreases to 0.21% under one-sun illumination. This is probably due to the enhancement of recombination of electron hole pairs. Further modification and optimization of the InN/TiO_2 system are expected in the next phase of studies.

3. The effects of anchoring groups – the linker between InN and TiO_2 (C. K. Wang and M. C. Lin)

We have carried out a series of studies on the effects of the linker or anchoring group between InN and TiO_2. Initially we employed the –OX(O)O- linker (X=B and P) by dipping the TiO_2 nanoparticle films, prepared by the sol gel method as described in sections (1) and (2), into the solution of H_3BO_3 and H_3PO_3 of varying concentrations.

InN deposition onto the treated films by PECVD after drying at about 100˚C in the deposition system under vacuum. Before turning on the microwave, the film was first dosed with TMIn to facilitate the formation of the first-layer chemical bond:

$$(CH_3)_3In + HOX(O)O\text{-}TiO_2 \rightarrow (CH_3)_2InOX(O)O\text{-}TiO_2 + CH_4\ (g)$$

where X=B or P and the $HOX(O)O\text{-}TiO_2$ has been shown by our quantum calculations using VASP to be the key products of the $X(OH)_3$ dissociative adsorption on TiO_2 anatase and rutile surfaces.

Following the TMIn dosing and pumping, the substrate was heated to 150˚C for PECVD of InN using NH_3 and TMIn as we previously reported to INER and in section (1). After PECVD, the fabricated $InN/OX(O)O\text{-}TiO_2$ devices were constructed for solar cell operations. The results summarized in Figure 11 clearly demonstrates that the electron-withdrawing B-element enhances, whereas the P-linker, diminishes the photo-efficiency.

This is a very important finding as both strongly binding linkers (to TiO_2 with >100 kcal/mol binding energies) can be used for other semiconductor quantum dots, for example, Si (using SiR_4), CdSe (using $Cd(CH_3)_2$), etc., as precursors to bind with $HOX(O)OTiO_2$.

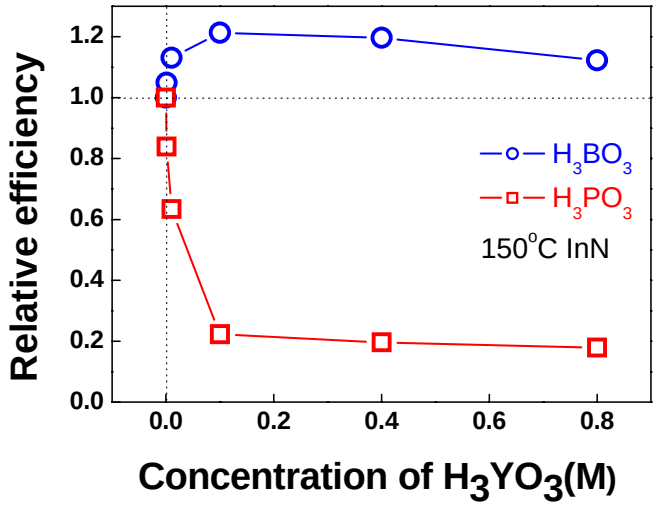

Figure 11. The effects of H_3BO_3 and H_3PO_3 as anchoring groups on photocurrent of InN/TiO_2.

Quantum chemical calculations to account for the observed B- and P- effects are under way.

四、New TiO_2 substrate preparation (C. W. Wu, M. C. Lin and Y.-P. Lee)

We attempted to prepare TiO_2 nanorods by the direct oxidation Ti foils as described Peng et al. [1] We washed titanium foils with distilled water and acetone in ultrasonic cleaner in 10 min. before employing hydrochloric acid (80°C, 30 wt%) to etch oxidized layer on surface of titanium foil. Subsequently, we removed residual hydrochloric acid on titanium foils with distilled water before putting the cleaned titanium foils into our reaction system.

The reaction system consists of two parts (see Figure 12): (1) a gas inlet for two different gases, He carrier gas and oxidant gas. (2) a quartz reaction tube of 5 cm diameter. The quartz tube was heated by a furnace with temperature up to 850 °C, followed by passing

various oxidants into the tube to oxidize Ti foil and produce TiO_2 nanorods (see Figure 13). After oxidation, the film of TiO_2 nanorods was deposited with InN by PECVD, as described in section (1).

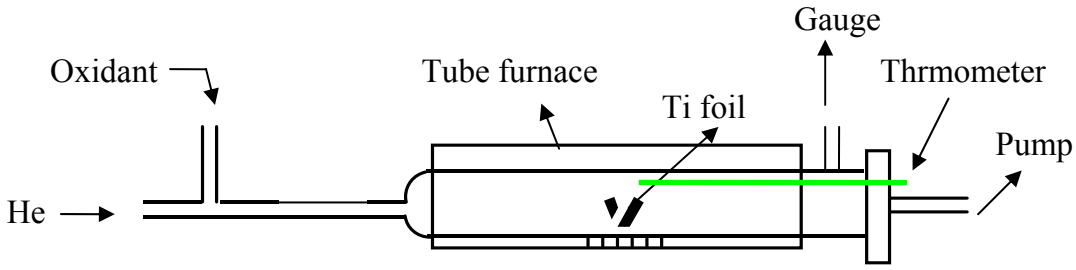

Figure 12: Schematic diagram of the Ti foil oxidation system.

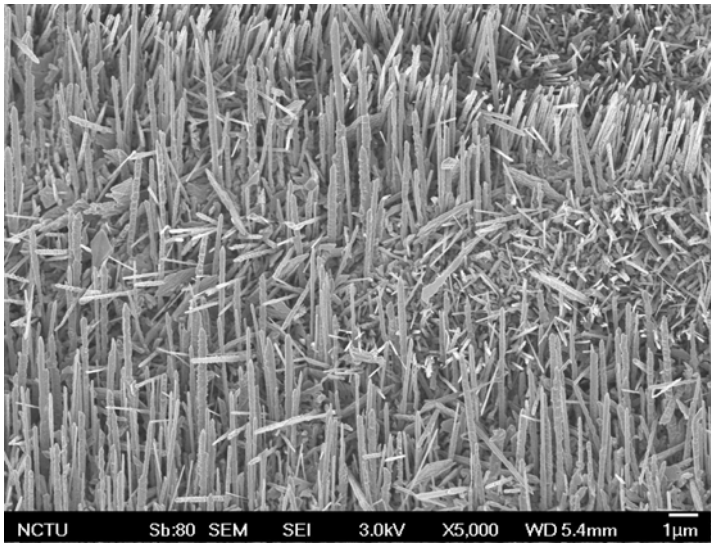

Figure 13: SEM images of TiO_2 nanorods prepared by flowing ~0.3 Torr 2-propanol and ~75 sccm of He into quartz reaction tube at 850°C for 2 h. The lengths of nanorods are ~2−3 μm and the diameters are ~100 nm.

The photo-efficiency of the InN/TiO_2-nanorod device, which is dominated by TiO_2 rutile structure, is relatively low at present. Currently we are exploring the effects of nanorods' height and

spacing as well as the type of the HOY(O)O- (Y=B and P) linkers, on the overall efficiency. This work is still in its infancy, we expect the technique to be able to fabricate a robust InN/TiO_2 photo-electrode for potential water-splitting applications.

References:

1. X. Peng, J. Wang and A. Chen, Nanotech., 2005, 16, 2389

參、主要發現與結論

在這一年利用 PECVD (NH_3+TMIn)及 OMCVD (HN_3+TMIn)的實驗結果，與目前 NREL 之 Nozik 實驗室在 2006 年發表的 InAs/TiO_2 結果很接近(見下圖）：

J. Phys. Chem. B 2006, *110*, 25451−25454 25451

Nanocrystalline TiO_2 Solar Cells Sensitized with InAs Quantum Dots†

Pingrong Yu,*,‡ Kai Zhu, Andrew G. Norman, Suzanne Ferrere, Arthur J. Frank, and Arthur J. Nozik*

Center for Basic Sciences, National Renewable Energy Laboratory, Golden, Colorado 80401

Received: July 27, 2006; In Final Form: September 29, 2006

We report nanocrystalline TiO_2 solar cells sensitized with InAs quantum dots. InAs quantum dots of different sizes were synthesized and incorporated in solar cell devices. Efficient charge transfer from InAs quantum dots to TiO_2 particles was achieved without deliberate modification of the quantum dot capping layer. A power conversion efficiency of about 1.7% under 5 mW/cm² was achieved; this is relatively high for a nanocrystalline metal oxide solar cell sensitized with presynthesized quantum dots, but this efficiency could only be achieved at low light intensity. At one sun, the efficiency decreased to 0.3%. The devices are stable for at least weeks under room light in air.

(A)

InAs/TiO_2 InN/TiO_2

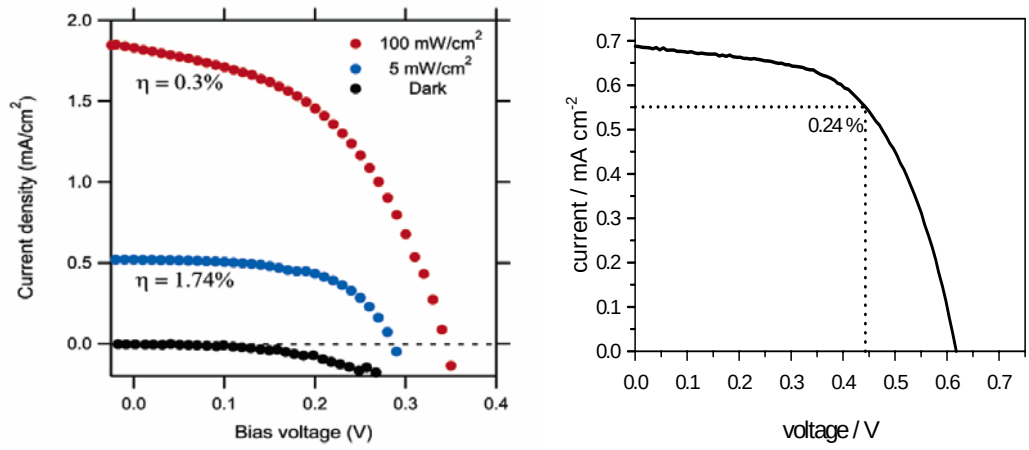

(B)

InN/TiO_2 與 InAs/TiO_2 目前結果的比較： (A) Nozik 等 2006 年 InAs/TiO_2 論文的摘要，(B) InAs 與 InN 的光電效率比較。

吾人利用高溫 PECVD 及 OMCVD 所製成的 InN/TiO_2 當然比 Nozik

等利用水溶液低溫物理吸附、並有化學毒性的 InAs/TiO_2 系統在物性與化性上均好得很多。此兩種量子點太陽能系統目前效率不高的原因至少有二：(1)依前述 SEM 分析結果，InN 或 InAs 量子點無法如有機染料分子一樣進入 TiO_2 奈米薄膜的內部孔洞，因此量子點濃度不高，(2)量子點(InN 或 InAs)與 TiO_2 奈米粒子表面尚未有良好、有效傳遞電子的化學鍵(諸如染料分子所用的-C(O)O-鍵）。

為解決上述第(2)點，吾人已在-OY(O)O-, Y=B 或 P，接鍵的實驗結果發現，-OB(O)O-與 TiO_2 連接對光電流有明顯的幫助，但同樣能與 TiO_2 強力接連的-OP(O)O-鍵則有明顯的負作用，這是非常重要的實驗結果，因為-OB(O)O-能與其他很多的半導體量子點，諸如 InP, Si, CdSe 等等，利用化學反應接連在 TiO_2 奈米點薄膜上。

有關以上第(1)點的改善，目前已在兩方面進行：(A)直接利用 Ti-foils 製作 TiO_2 nanorods (如 section (4)所述)，達成廣大的孔洞；(B)利用 glycine nitrate 的方法在 TiO_2 奈米薄膜的上層製作大孔洞。同時在 TiO_2 奈米粒子中加入 n-或 p- dopants 的實驗已進行中，此外，半導體敏化的量子點本身亦可加入 n-或 p-dopants，諸如 Zn 或 Sb 等。

吾人確信將來在敏化量子點(sensitizer)、量子點與 TiO_2 奈米粒子的接連化學鍵 (linker or anchoring group)及 TiO_2 奈米薄膜的 n-或 p-doping 三方向的調製與改進，一定可以製作一個高效率的 In(M)N/Linker/d-TiO_2 系統 (M=Zn, Ga, Sb…; Linker = OY(O)O, Y= B, P, Si, Al…; d= n- or p-dopants)，以供太陽光水分解之應用。

Resulting publications:

1. C.-W. Chang, C. K. Chou, I-J. Chang, Y.-P. Lee and E. W.-G. Diau, "Relaxation Dynamics of Ruthenium Complexes in Solution,

PMMA and TiO_2 Films: The Roles of Self Quenching and Interfacial Electron Transfer", J. Phys. Chem. C, 2007, 111, 13288

2. A. M. Kechiantz, K. W. Sun, H. M. Kechiyants and L. M. Kocharyan, "Strong Barrier Effect on the Conversion Efficiency of Solar Cells with Buried Type-II Quantum Dots", Semiconductor Science and Technology, 2007, 22, 616
3. C.-W. Wu, Y.-F. Lu, Y.-C. Liu, C.-H. Chiou, Y.-P. Lee and M. C. Lin, "Nanocrystalline TiO_2 Solar Cells Sensitized with InN Nanoparticles Produced by Plasma-enhanced Chemical Vapor Deposition", submitted to Phys. Chem. Chem. Phys. (PCCP)
4. C.-S. Lee, S.-Y. Chen and M. C. Lin, "Synthesis of $In(OH)_3$ and In_2O_3 Nanomaterials Incorporating Au", Submitted to Inorg. Chem.
5. M.-C. Wu and C.-S. Lee, "A New Deposition to Prepare a Thin Film of Quasi-Aligned-MoO_3 Nanorods", Submitted to Thin Solid Films
6. T.-T. Wang, Y.-F. Lu, Y.-C. Liu, C.-H. Chiou and M. C. Lin, "Nanocrystalline TiO_2 Solar Cells Sensitized with InN Nanoparticles Grown by Organometallic Chemical Vapor Deposition", in preparation.